EUROPEAN FUSION DEVELOPMENT AGREEMENT

EFDA–JET–PR(03)25

M.E.Puiatti, M.Valisa, M. Mattioli, T. Bolzonella, A. Bortolon, I.Coffey, R.Dux,
M.von Hellermann, P.Monier-Garbet, M.F.F.Nave, J.Ongena
and JET EFDA contributors

Simulation of the Time Behaviour of Impurities in JET Ar-Seeded Discharges and its Relation with Sawtoothing and RF Heating

Simulation of the Time Behaviour of Impurities in JET Ar-Seeded Discharges and its Relation with Sawtoothing and RF Heating

M.E.Puiatti[1], M.Valisa[1], M. Mattioli[1], T. Bolzonella[1], A. Bortolon[1], I.Coffey[2], R.Dux[3], M.von Hellermann[4], P.Monier-Garbet[5], M.F.F.Nave[6], J.Ongena[7] and JET EFDA contributors*

[1]Consorzio RFX, Associazione Euratom-ENEA sulla Fusione, Padova, Italy
[2]Queens University, Belfast BT7 INN, North Ireland
[3]Max-Plank Institut fur Plasmaphysik, EURATOM Association, D-8046 Garching, Germany
[4]FOM Instituut voor Plasmafysica Rijnhuizen, EURATOM Association, Nieuwegein , The Netherlands
[4]Association Euratom-CEA, DRFC, CEA Cadarache, St Paul lez Durance, France
[5]Associacao Euratom-IST, Centro de Fusao Nuclear, Lisboa, Portugal
[6]LPP-ERM/KMS Euratom-Belgian State Association, Brussels, Belgium
** See annex of J. Pamela et al, "Overview of Recent JET Results and Future Perspectives", Fusion Energy 2000 (Proc. 18th Int. Conf. Sorrento, 2000), IAEA, Vienna (2001).*

Preprint of Paper to be submitted for publication in
Plasma Physics and Controlled Fusion

ABSTRACT.

In JET, Ar seeding has proven to be a successful means to reach quasi-stationary regimes that feature, simultaneously, high density, high confinement and an edge radiation belt without significant contamination of the plasma. A detailed analysis shows that in presence of centrally deposited Ion Cyclotron Resonance Heating Ar transport increases. Sawteeth also hamper the accumulation of Ar in the core, though their contribution is less relevant compared to the effect of the ICRH. The transport increase associated to the RF injection appears as a reduction of the inward pinch convection. The analysis is carried out by means of a 1D impurity transport code, which has been applied to several Ar-seeded discharges. The result about the role of sawteeth is independent on triangularity. In the high triangularity discharges, with continuous D refueling, the convection of impurities in the core region is typically very small so that ICRH injection itself has little relevance in the control of the Ar behaviour.

INTRODUCTION

ELMy H-mode discharges have been extensively studied on JET. A general finding is that when the electron density approaches the Greenwald limit confinement deteriorates and falls below the H-mode confinement scaling [1]. Among the methods devised to reduce such performance degradation Ar seeding has proven successful to maintain high confinement values at densities close or even exceeding the Greenwald limit [2, 3, 4]. In addition, Ar-seeded discharges feature a poloidally and toroidally uniform radiative mantle and a reduced thermal load on the divertor plates. This is important in view of ITER, where, due to the high levels of input power, heating and erosion of the first wall will be a critical issue.

The presence of Ar in high perfomance discharges imposes a particular attention to the contamination of the core, which is to be kept under control to avoid detrimental central radiation losses.

Different phenomena influence the impurity concentration in the core: transport processes, both in the core and at the edge, as well as the impurity injection rate. A sufficiently low diffusion and/or an inward convective velocity may induce a peaking of the impurity profiles higher than the density peaking, thus resulting in an impurity accumulation process. On the other hand, to avoid accumulation the impurity influx has to be kept below a critical threshold. Transport properties of the edge are particularly important: high edge diffusivity or the presence of ELM's typically favour the expulsion of the impurities.

Previous studies about the Ar transport in JET seeded discharges have been reported in [5]. The main result was that the accumulation of Ar can be avoided in presence of sawteeth and/or of moderate central Ion Cyclotron Resonant Heating (ICRH) as reported in [6] and [7], as well as adopting high triangularity magnetic configurations. However, the role of ICRH and that of sawteeth was not deconvolved.

The importance of sawteeth in shaping the impurity density profiles depends on their frequency, on the fraction of the plasma volume affected as well as on the transport properties of the discharge. For instance, the capability of sawteeth of expelling impurities can be important to balance a significant

inward convection term [8]. Impurities themselves with the associated radiative losses can affect the amplitude of the sawteeth by draining power from the core between sawtooth crash [9].

The aim of this paper is to understand to what extent the avoidance of Ar peaking in JET seeded discharges may be the consequence of the sawteeth maintenance when moderate central ICRH is applied [7]. For this purpose, several H-mode Ar seeded discharges, with and without ICRH, have been simulated and the details of the sawteeth behaviour have been analysed. In section 2 the experimental scenario is presented. The method of the impurity transport analysis is described in section 3. In sec. 4 the specific analysis of the impurity behaviour resulting from the presence of sawteeth is presented and finally in section 5 some conclusions are drawn.

1. EXPERIMENTAL SCENARIO: LOW TRIANGULARITY DISCHARGES

Argon seeded plasma discharges, with and without ICRH, have been analyzed both in low and high triangularity magnetic configuration. In this section, two low triangularity discharges (0.25 lower triangularity, 0.18 upper triangularity) selected for the analysis, with and without ICRH, are described. The two discharges have comparable $B_t \sim 2.5$T, $I_p = 2.5$-2.7MA, $q_{95} = 3.05$ and refer to a septum configuration, where the X point of the magnetic separatrix sits on the dome of the divertor. The main parameters of the discharges are shown in fig.1.

The experiment commences by puffing in ELMy H-mode plasma deuterium and Ar simultaneously, to increase the electron density. In this phase of about two seconds, dubbed "inflow phase" (IP), the temperature and the confinement factor H97 drop. When gas puffing is suddenly reduced to the much smaller rates required to maintain the density (after-puff phase, AP) temperature and confinement factor recover despite the higher density. This good confinement phase is maintained quasi-stationary for about 10 confinement times. In discharge Pulse No: 52146 ~2MW of ICRH heating deposited at the plasma center are added to the neutral beam heating power, resulting in a slightly higher on-axis electron temperature. The profiles of electron temperature and electron density for both discharges during the IP and the AP are shown in fig.2. In Pulse No: 52146 the temperature profile during the AP phase is more peaked, while the density is lower and slightly flatter. According to the neoclassical transport theory, this implies a reduced impurity peaking for the Pulse No: 52146, since the peaking factor v_{neo}/D_{neo} is roughly proportional to $Z\,(\nabla n/n - \alpha \nabla T/T)$, with the a factor ranging between 0.2 and 0.5 [10]. The after-puff phase starts at t~2s. The evolution of the profiles of the SXR emissivity, dominated by the highly ionized Ar ions, and of the Ar^{18+} densities from charge-exchange measurements are shown in fig.3a,b. In Pulse No: 52136 during the AP the SXR emissivity increases and peaks, while in Pulse No: 52146 it decreases first and then remains constant. Since the decrease of the density is modest (from 8×10^{19} m^{-3} to 7×10^{19} m^{-3}) and the temperature increases, the SXR behaviour in discharge Pulse No: 52146 suggests a decrease of the on-axis Ar density. This tendency is confirmed by the CX measurements, though the innermost experimental point is at r/a~0.18. Therefore the difference in the experimental evolution of the Ar radiation in the two shots is essentially localized in the central region, with a more pronounced peaking of the profiles in the pulse without ICRH.

Carbon behaves differently: as shown in fig. 3c. In both pulses the C^{6+} density profiles are maintained hollow throughout the AP phase and do not show peaking processes.

The on-axis SXR emissivities (fig.4) show that the sawtooth behaviour is different in the two discharges. In Pulse No: 52136, without ICRH, sawteeth are suppressed at about 3.5s during the AP. In discharge Pulse No: 52146, with ICRH, a well defined sawtooth activity (ST) is maintained during both IP and AP phases. The SXR emissivity increases during the IP and then, correspondingly to a much lower Ar influx, decreases during the AP. However, when the SXR behaviour in the two discharges begins to differentiate, a ST activity is still present in both of them.

For discharge Pulse No: 52146 figure 4 shows a ST inversion between the inflow and the after-puff phase: the SXR signal at the ST crash increases during the IP and decreases during the AP. The former situation may be interpreted as Ar penetrating in the plasma centre, the latter one as an expulsion of Ar from the core. In Pulse No: 52136, the same ST inversion is observed at earlier times than in Pulse No: 52146, indicating that ~1s after the start of IP a consistent amount of Ar is already present in the plasma centre.

2. IMPURITY TRANSPORT MODELLING

The interpretation of the data has been carried out by means of a 1D cylindrical impurity transport model coupled to a collisional-radiative model [11]. The radial transport of the ions of the species with atomic number Z_N is described by solving the system:

$$\partial n_z/\partial t = -1/r \cdot \partial(rG_z)/\partial r + n_e\,(n_{z-1}S_{z-1} - n_z S_z + n_{z+1}a_{z+1} - n_z a_z) \qquad (1)$$

with $Z=1,..Z_N+1$ and where the radial ion flux G_Z is expressed in terms of a diffusion coefficient D and a pinch velocity v (v >0 corresponds to outward velocity), assumed independent of the ion charge:

$$\Gamma_Z\,(r) = -D(r)\,\partial n_Z(r)/\partial r + v(r)\,n_Z(r) \qquad (2)$$

The atomic coefficients in (1), where S_Z are the ionization rates for the ions of charge Z and α_Z are the radiative plus dielectronic plus charge-exchange recombination rates, have been discussed in Refs [11, 12]; they depend on the electron temperature and density profiles, input data to the code. The impurity influx is given as boundary condition, supposing that impurities enter the plasma at the last mesh (~5cm outside the LCFS) as neutrals with a velocity of 5×10^3 m/s corresponding to 5eV for Ar. However this value has negligible influence on the simulation. The time evolution of the influx is prescribed by tracking the peripheral line brightness time evolutions of Ar VII and C III respectively.

The transport coefficients D and v are radius and time dependent and are chosen in such a way as to obtain the best simulation of the available experimental data. In particular, for the determination of the Ar core transport parameter, due to the uncertainties associated to the CX Ar cross-sections. SXR data have been considered with the higher weight together with the Zeff value. In the edge

region the determination of the transport coefficients derives mainly from the simulation of the line emission spectra in the spectral region between 20 and 0 Å, featuring lines from Ar XIII to Ar XVI that populate the plasma periphery.

In all the simulations the diffusion profile has been found to decrease towards the plasma centre. It can be observed that a similar shape of D is obtained by the evaluation of the anomalous diffusion associated to ion temperature gradient plus dissipative trapped electron instabilities, as reported for example in [13]. The transport coefficients for carbon have been determined by reproducing the CX data in the core and the C V and C VI spectral line brightness at the edge.

The calculation accounts for the non-circular plasma shape by replacing r with the function V' in the diffusion term ($V' = dV_p(r)/dr$, with V_p volume inside the magnetic surface of radius r) [14].

3. ANALYSIS OF SAWTEETH

First we report the results of the simulations of the impurity transport in-between sawteeth in the two discharges presented in section 2; then the effect of sawtooth crash will be discussed

3.1. TRANSPORT ANALYSIS IN-BETWEEN SAWTEETH

Figure 5 shows the diffusion coefficient and convective velocity obtained in the IP phase from the simulation of Ar and carbon. The diffusion coefficient of Ar is the same in the two discharges: D = 0.75 m^2/s in the external half of the plasma, decreasing to D=0.15 m^2/s in the centre. To get a good agreement between the experimental and simulated line emission spectra a low diffusivity and high an inward velocity at the edge (r>0.95) are required, as found also in previous simulation of JET spectra [11]. The convective velocity of Ar in the main plasma is outward throughout the IP in Pulse No: 52146, while in Pulse No: 52136 it becomes inward for t≥1s. This results in a difference of the Ar density radial profiles and of the SXR emissivity at the end of the inflow phase (t = 2s), as shown in figures 6a and 6b: some Ar peaking process in discharge Pulse No: 52136 has already started before the AP phase begins.

For carbon, the diffusion coefficient is the same one adopted for Ar, but to reproduce the high experimental value of the ratio r ~4 between the brightness of the Ly_α (33.7Å) C VI and the resonance (40.23Å) C V line, the edge diffusion barrier found for Ar is not sufficient. A higher velocity, inward directed, in the last 0.2 m of the plasma radius has to be prescribed.

During the AP phase, the difference between the two discharges in terms of transport parameters is more pronounced (fig.7). The diffusion coefficient is the same for both, but a much higher inward pinch velocity is found in Pulse No: 52136. Fig. 8 shows the total Ar and the Ar^{18+} density and the SXR profiles obtained from the simulations of the two discharges, with the experimental curves reported for comparison.

The opposite choice of a constant inward pinch and a different diffusion level is not equivalent; simulations of Pulse No: 52136 fixing v and varying D but keeping the same peaking parameter (v/D), result in SXR and CX density profiles much flatter than the experimental values. A high inward velocity is therefore needed to simulate discharge Pulse No: 52136.

Carbon is not influenced by the decreased Ar puffing rate during AP, since its transport coefficients do not change with respect to the IP in both discharges. As in the IP, also in the AP the simulation of the line emission spectra leads to different external transport barriers for C and Ar. A detailed study of the effect of the mass and charge of impurities on their transport parameters in Ar seeded discharges will be the object of a separate experiment, including the analysis of high-Z element laser blow-off pulses; it is anyway a well known fact that mass and charge are a discriminating parameter in terms of impurity transport [15].

The calculated time evolution of the Ar XVI line and of the SXR brightnesses are compared in figs. 9a and 9b with the experimental ones for the two analyzed discharges. The neoclassical transport coefficients of Ar (banana-plateau [16] plus Pfirsh-Schluter [17]) have been evaluated for the two discharges including the collisions with deuterium and carbon. In the plasma centre the Ar diffusion coefficients resulting from the simulations are about 3 times the neoclassical values. The neoclassical (inward) velocity is found much higher than the one simulated in Pulse No: 52146 and only a factor two higher in Pulse No: 52136.

3.2 EFFECT OF THE SAWTOOTH CRASH

In Pulse No: 52146, where 2MW of central ICRH are applied, the ST are maintained both in the IP and in the AP, while in Pulse No: 52136 in the AP ST show at first a higher frequency and a larger amplitude and then are suppressed. The difference in impurity behaviour between the two discharges starts at the beginning of the AP, when the ST activity in Pulse No: 52136 has not been suppressed yet. This finding already suggests that in these discharges sawteeth do not have an exclusive role in the control of the impurity profiles.

The ST crashes have been simulated during both the IP and the AP phases by assuming in the calculation a discontinuity in the diffusion coefficient, increased up to 50 m^2/s in the central region. During the IP in Pulse No: 52146, due to the hollow Ar profiles, the enhanced diffusion associated to each ST crash leads to a progressive penetration of Ar in the plasma core, since the contribution due to the enhancement of the central diffusion dominates on the effect of the decreased temperature. Both simulated and experimental SXR data just before and after a ST crash are shown in fig. 10. Instead, in Pulse No: 52136 the ST are associated to a penetration of Ar only during the first second of the IP. Later, the Ar profile tends to peak and ST crashes tend to flatten the impurity profiles by ejecting Ar; the latter effect is in any case lost before the subsequent crash.

During the AP phase the density profiles of Ar highly charged ions are peaked also in Pulse No: 52146, and the enhanced diffusion corresponding to the crash has the effect of expelling Ar [7]. The simulated SXR profiles for the two analyzed discharges before and after a ST crash are compared with the experimental inverted profiles in fig.11. For both discharges the ST crash corresponds to a decrease of the on-axis SXR emissivity: the simulation of discharge # 52136 shows a tendency to over-estimate the effect of ST on the profile.

The influence of ST on the Ar concentration can be inferred from fig.12. In Pulse No: 52136 (without ICRH), despite the relatively large amplitude of the ST, the concentration of Ar increases

in time. In the discharge with ICRH the concentration decreases slightly during the AP. This indicates that in discharge Pulse No: 52146, with ICRH, ST correspond to a temporary expulsion of Ar from the plasma centre, but the time evolution of the central Ar concentration is determined by acore transport characterized by the relatively low inward pinch velocity documented in Fig.7.

The analysis has been extended to other low triangularity discharges with and without ICRH injection. Fig. 13 shows the on-axis SXR emissivity of three other low triangularity shots (one with 2 MW of ICRH and two without RF) together with the SXR of the two discharges analyzed above. The traces in the figure are numbered in order of increasing Ar injection rate. The sudden increase of the on axis SXR emissivity at the end of the IP in the discharges without ICRH is not justified in the simulation by the evolution of plasma temperature and density; it rather indicates the onset of an Ar peaking process, with the exception of discharge #52147. In the latter case the temperature drop at each ST crash is ~ 500 eV, higher than in the other discharges, and unlike the other discharges it contributes significantly to the slow decrease of the SXR central emissivity, adding its effect to the one produced by the flattening of the Ar density profiles at each sawtooth crash. The simulation still requires an inward pinch term in-between ST, though lower than in the discharges featuring Ar accumulation. The simulated evolution of the Ar density profile across a ST crash is shown in Fig. 14 together with those of discharges 52146 and 52136.

Fig. 12 also suggests an effect of the Ar influx rate on the accumulation process: in discharge Pulse No: 52147 the total injected neutral beam power is the same as in discharge Pulse No: 52148 (featuring a larger increase of the SXR emssivity after the IP), but the Ar puffing rate is the lowest. On the other hand it is known that Ar puffing does ultimately affect transport in the core, as indicated also by the drop in the core thermal diffusivity calculated by TRANSP in presence of Ar seeding [3].

In summary, sawteeth hamper the Ar accumulation process. However, when the Ar puffing rate is sufficiently high the expulsion of Ar due to sawteeth does not compensate the increased inward convection and Ar concentration builds up. The presence of centrally deposited ICRH reduces significantly the inward convection and can control Ar concentration in a way that in the cases examined here is more significant than that associated to sawteeth. Injection of centrally deposited ICRH has been found to be beneficial also in discharges with much higher Ar puffing rates allowing for a stronger radiation belt at the edge [7,5].

3.3 HIGH TRIANGULARITY CASES

The effect of ST has also been analyzed in discharges with higher triangularity (0.35 lower triangularity, 0.45 upper triangularity). The radiation patterns of discharge Pulse No: 53146 with ~2MW of central ICRH and discharge Pulse No: 53145 without ICRH, have been reconstructed by the impurity transport model. In these discharges B_t ~ 2.4T, I_p = 2.3MA, q_{95} = 3.08, P_{NBI}~15MW. High density levels can be maintained independently on the presence of Ar. The D_2 and Ar puffing schemes are shown in fig.15 for the Pulse No: 53146. The D_2 puffing rate is high throughout the discharge (as allowed by the high triangularity configuration). The Ar puffed into the plasma has relatively high rates with respect to the low triangularity cases examined above, but for shorter times.

As previously found for high triangularity configurations [5], the simulations of these discharges lead to very low values of the convective velocity, which during the AP are about zero or even slightly positive (outward).Unlike the low triangularity case, the application of ICRH does not affect significantly the Ar profiles. Both discharges, with and without ICRH, have been simulated with the same transport coefficients and do not show peaked Ar profiles (fig.16). We notice that besides the magnetic topology, another difference between the low and high triangularity discharges examined is the presence in the latter ones of continuous D_2 puffing; possibly the associated higher diffusivity at the edge could favour the Ar expulsion [13].The comparison of the experimental SXR profiles across ST crashes does not show any significant difference. For example, for shot #53146 the simulation of a sequence of three subsequent experimental ST is compared in terms of SXR profiles with the simulation in which the sawteeh have been removed. The only effect of the ST is to reduce the on-axis emissivity by ~5% (fig.17) while the effect on the Ar concentration is negligible.

CONCLUSION

In JET high performance Ar seeded discharges, Ar is likely to accumulate, especially in the low triangularity configuration. Accumulation is in general not observed when moderate amount of centrally deposited ICRH is injected. The aim of the paper was to discriminate if the different behaviour of Ar can be ascribed to the sawteeth maintenance associated to the RF injection or to a different transport associated to the presence of ICRH. A 1-dim impurity transport model has been applied and a detailed simulation of the time evolution of the Ar concentration in several discharges has been carried out. The main result of the analysis is that ST do influence the Ar density profile by expelling particles from the core during the after puff phase, but their role in the avoidance of accumulation is modest in the discharge with ICRH. RF injection increases the Ar transport in-between ST thus flattening the Ar density profiles. In the discharges without ICRH and affected by impurity accumulation analyzed in this paper, Ar shows the tendency to peak at the very beginning of the after puff phase, when the ST activity is still present but is unable to contrast the inward convection. The analysis of low triangularity discharges with different Ar puffing rates and different levels of neutral beam power confirms that the addition of centrally deposited ICRH is a robust technique to maintain flat Ar density profiles with low radiation from the plasma centre. Non-accumulating discharges can be obtained also without ICRH provided enough NBI power and a carefully dosed Ar puffing are operated. However the addition of ICRH appears to be more effective, allowing for higher Ar puffing rates [7]. It can be observed that also in ref [9] the onset of impurity accumulation in TEXTOR has not been related to the sawtheeth activity.

In high triangularity discharges with continuous puffing, flat Ar profiles can be more easily maintained both with and without the injection of ICRH, because the impurity transport is intrinsically characterized by a lower peaking factor (v/D). For the same reason in the high triangularity experiments the ST activity has not an important role in determining the Ar profiles, which are in any way flat. Finally, it has to be mentioned that the diffusion coefficient empirically determined by these simulations is in very good agreement with that reported in ref. [18] for JET L-mode

plasmas deriving from the calculation of the ITG and DTE instabilities, calculated according to [13]. This agreement provides a good starting point for the interpretation of impurity transport in the context of a theoretical model.

REFERENCES

[1]. Suttrop W., et al., Phys. of Plasmas **9** (2002) 2103

[2]. Dumortier P et al., Plasma Phys. Control. Fusion **44** (2002) 1845

[3]. Ongena J. et al., Phys.Plasmas **8** (2001) 2188

[4]. Maddison G.P., et al., Nucl. Fusion **43** (2003) 49

[5]. Puiatti M.E., et al., Plasma Phys. Control. Fusion **44** (2002) 1863

[6]. Van Oost G., Messiaen A.M., Phillips V. et al., Proc. 22nd EPS Conf. on Contr. Fusion and Plasma Phys., Bournemouth 1995, part III,p.345

[7]. Nave, M.F.F., et al., accepted for publication in Nucl. Fusion

[8]. Seguin F.H. and Petrasso R., Phys Rev. Lett., **51** (1983) 455

[9]. Tokar M.Z., Rapp J. , Bertschinger G. et al, Nucl. Fus., **37** (1997) 1691

[10]. Dux R. Giroud C., Neu R.,et al., Jour. Of Nucl. Mat., 313-316 (2003) 1155

[11]. Mattioli M. et al., Jour. Of Phys. B : At.Mol.Opt.Phys.34 (2001) 127

[12]. Mattioli M., et al., , Plasma Phys. Control. Fusion **44** (2002) 33

[13]. Kalupin D, Tokar M.Z., Dumortier P., et al., Plasma Phys. Control. Fusion **43** (2001) 945

[14]. Hinton F.L., Hazeltine R.D., Rev. mod. Phys. **48** (1976) 239

[15]. Dux R., Peeters A.G., Gude A., et al., Nucl. Fus. **39** (1999) 1509

[16]. Hawryluck R., Suckewer S.,Hirshman S.P., Nucl. Fus **19** (1979) 607

[17]. Hirshman S.P., Sigmar P.J.,Nucl. Fus 21 (1981) 1079[18] Tokar,M.Z., et al., Plasma Phys. Control. Fusion **44** (2002) 1903

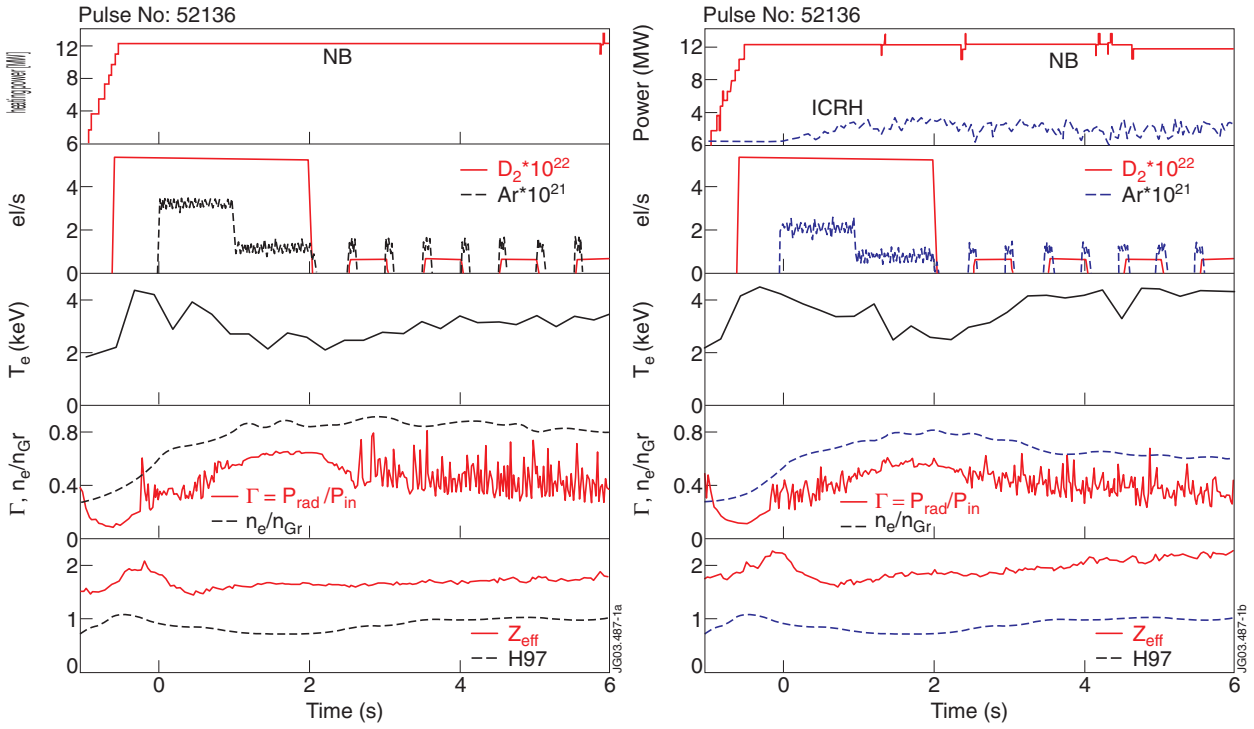

Figure 1: Main plasma parameters of the low triangularity pulses Pulse No: 52136 and Pulse No: 52146. From top to bottom: neutral beam and RF heating power; D_2 and Ar fluxes; on-axis electron temperature; radiation fraction (P_{rad}/ P_{inp}), Greenwald factor (n_e/n_{Gr}); effective charge and confinement factor f_{H97}. Times are referred to the start of Ar puff.

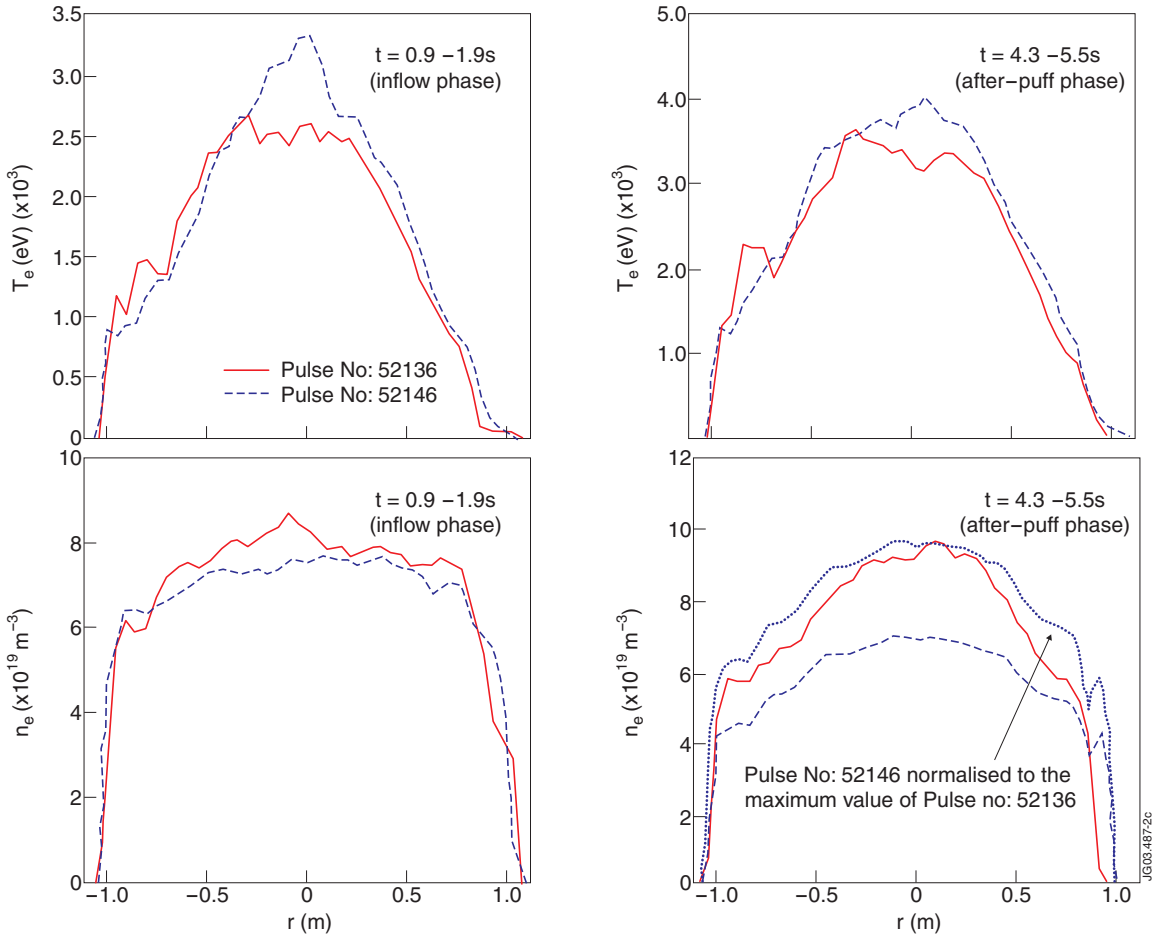

Figure 2: Electron temperature and density profiles at t=1s (inflow phase) and t=3s (after-puff phase) in the low and high triangularity discharges of the previous figure as obtained by the core Lidar scattering.

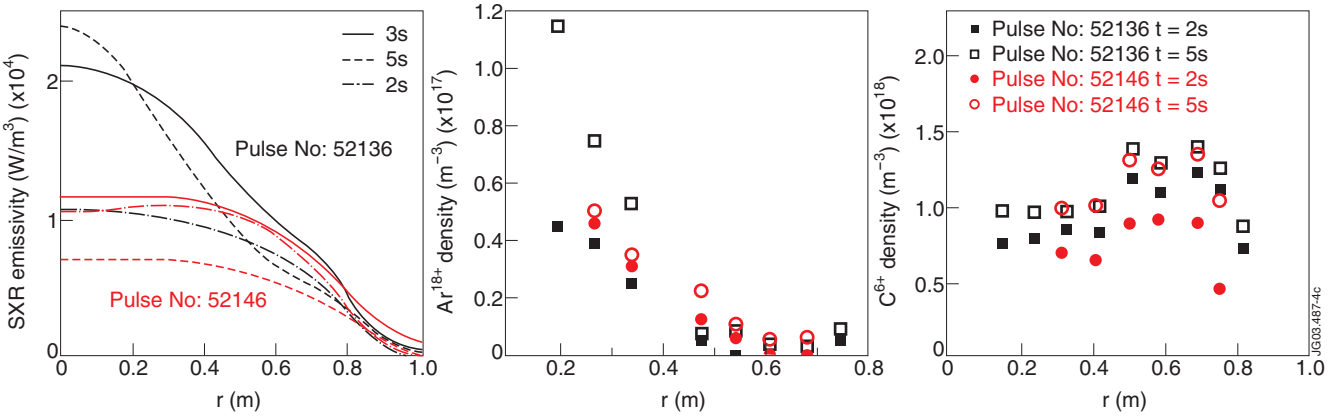

Figure 3: Comparison of pulses Pulse No: 52136 and 52146 in terms of the time evolution of (a) experimental Abel-inverted soft X-ray emissivity profiles (b) Ar^{18+} profiles from charge-exchange measurements and (c) experimental C^{6+} profiles from charge-exchange.

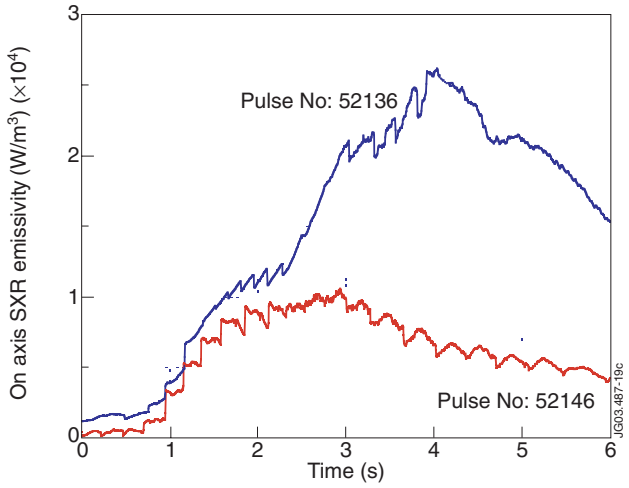

Figure 4: time evolution of the inverted on-axis soft X-ray emissivity in the two pulses Pulse No's: 52136 and 52146.

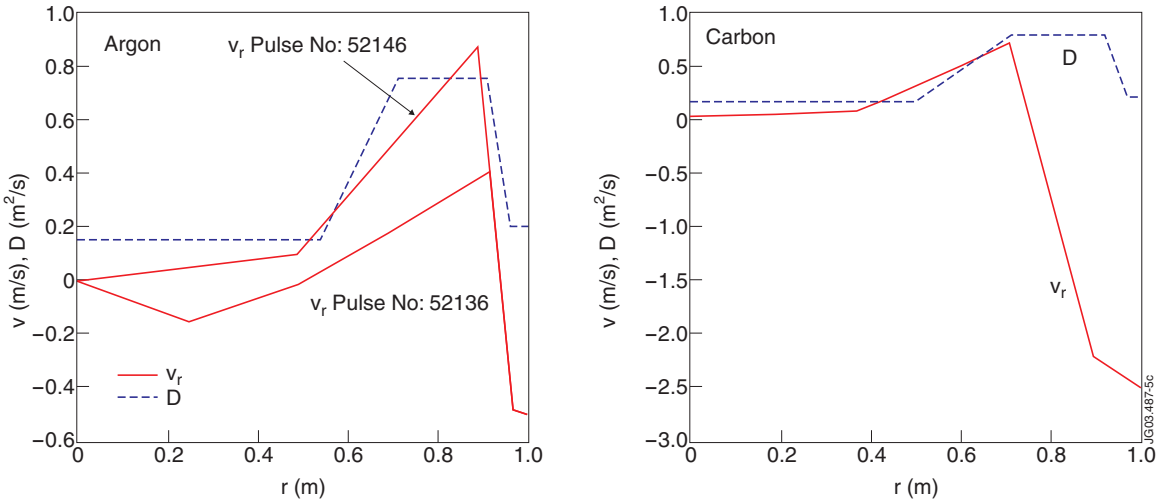

Figure 5: Ar and carbon transport parameters during the inflow phase.

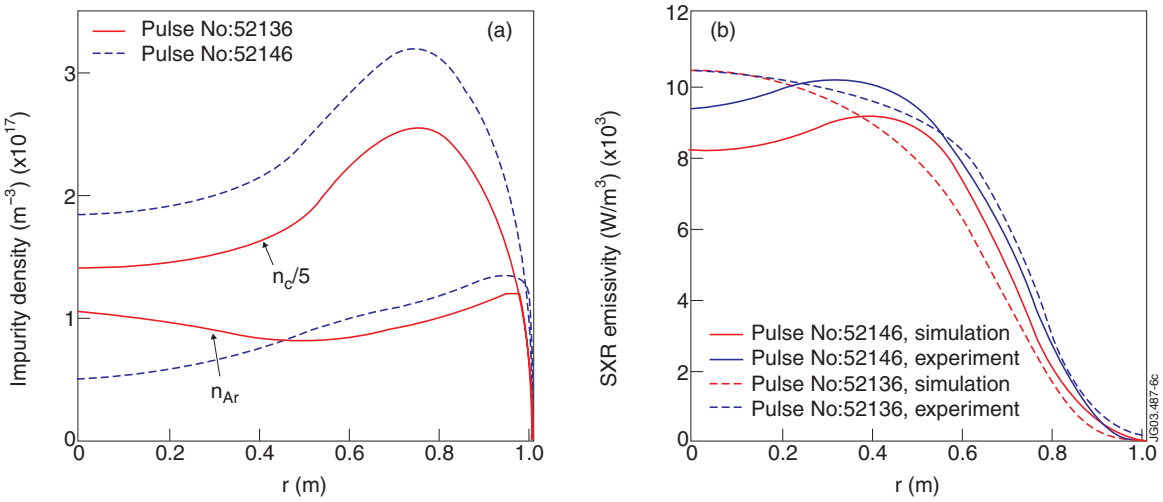

Figure 6: Comparison of the Ar and C density profiles and of the soft X-ray emissivities as obtained from the simulation of the two discharges during the inflow phase. The experimental profiles are also shown.

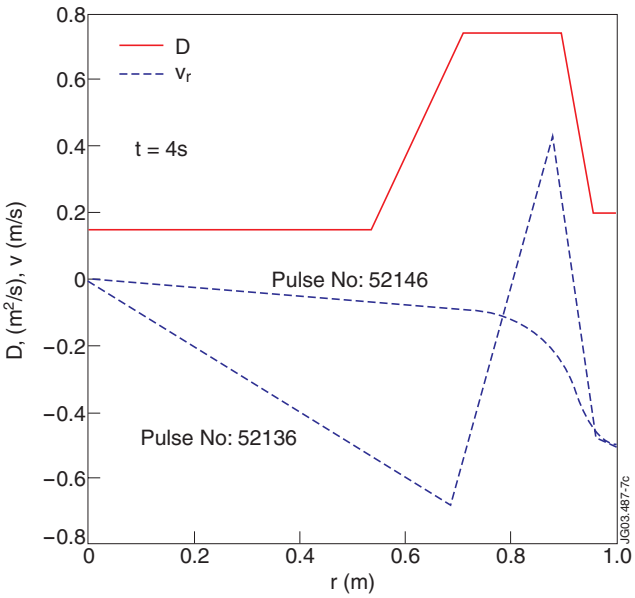

Figure 7: Ar transport parameters during the after-puff . The diffusion coefficient is the same for both discharges.

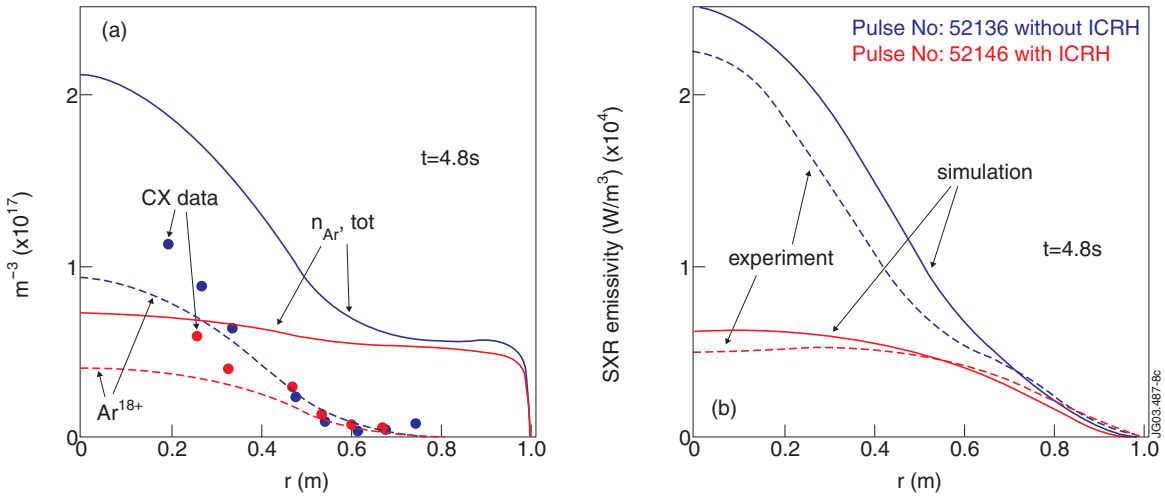

Figure 8: (a) total Ar and Ar^{18+} density profiles during the after-puff for pulses Pulse No: 52136 and Pulse No: 52146 as obtained from the simulation. The charge-exchange data are also reported. (b) Experimental and simulated soft X-ray emissivity profiles

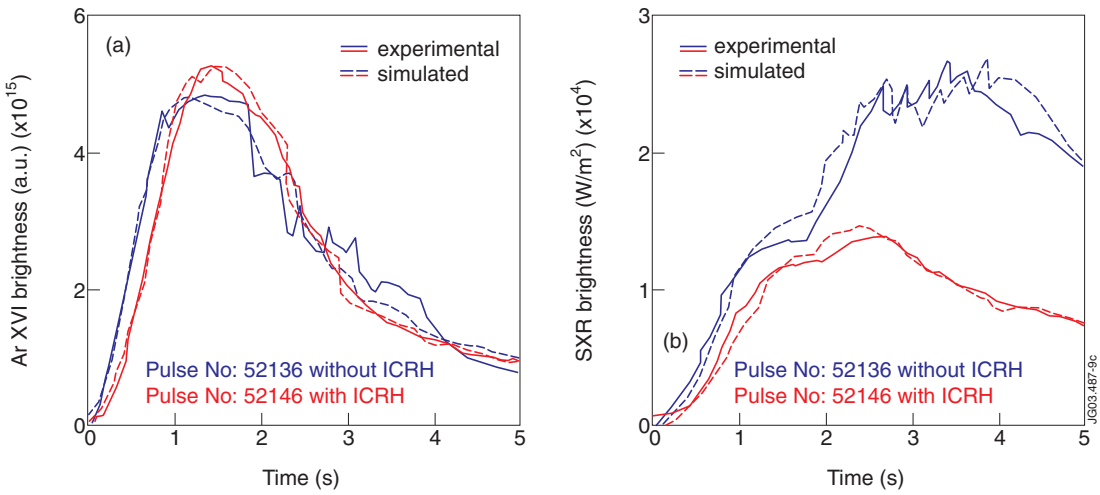

Figure 9: Simulation of the time evolution of the Ar XVI 354Å line (a) and of the soft X-ray (b) brightness in the two analyzed low triangularity discharges.

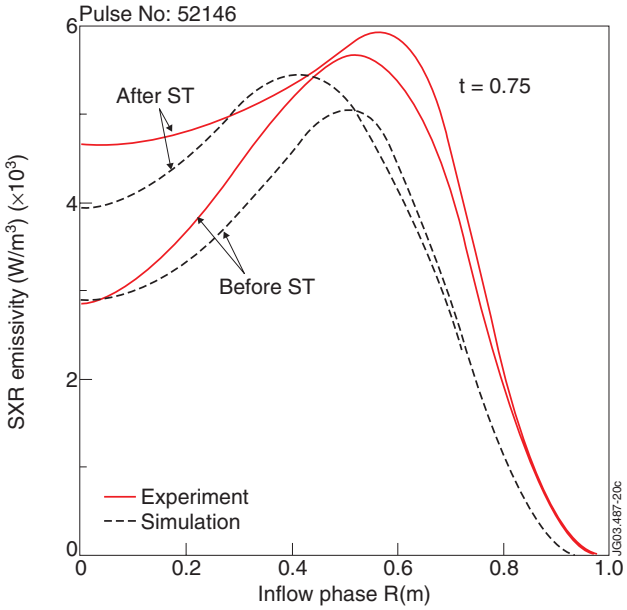

Figure 10: Effect of sawteeth during the inflow phase: simulated and experimental soft X-ray profiles.

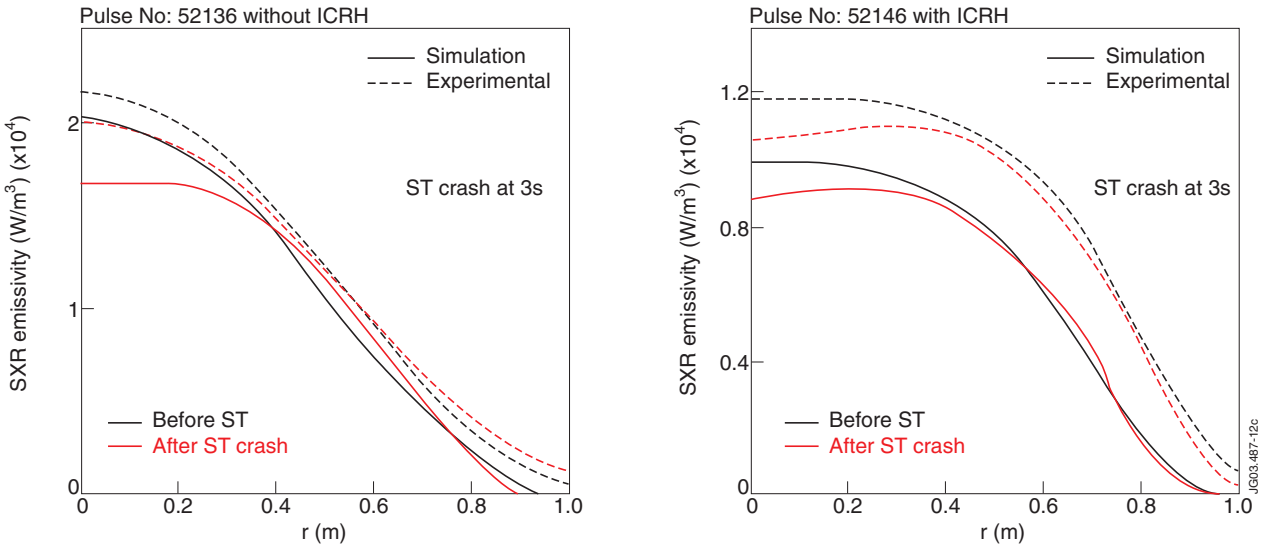

Figure 11: Effect of sawteeth during the after-puff phase: simulated and experimental soft x-ray profiles before and after a sawtooth crash: (a) Pulse No: 52136 without ICRH; (b) Pulse No: 52146 with ICRH.

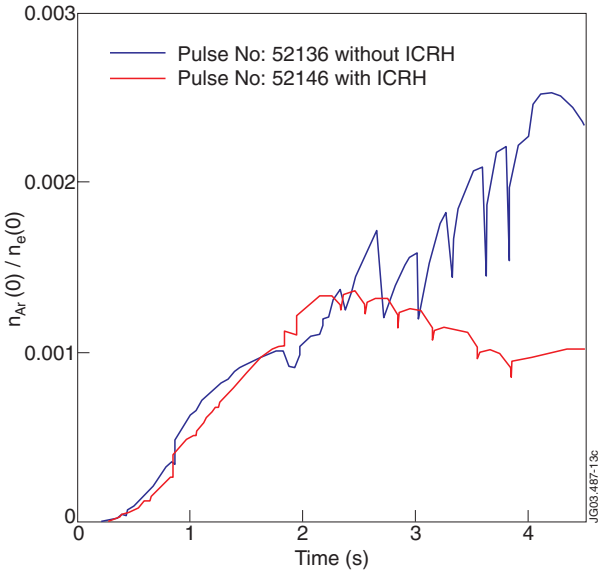

Figure 12: Time evolution of the on-axis Ar concentration for Pulse No's:52136 and 52146

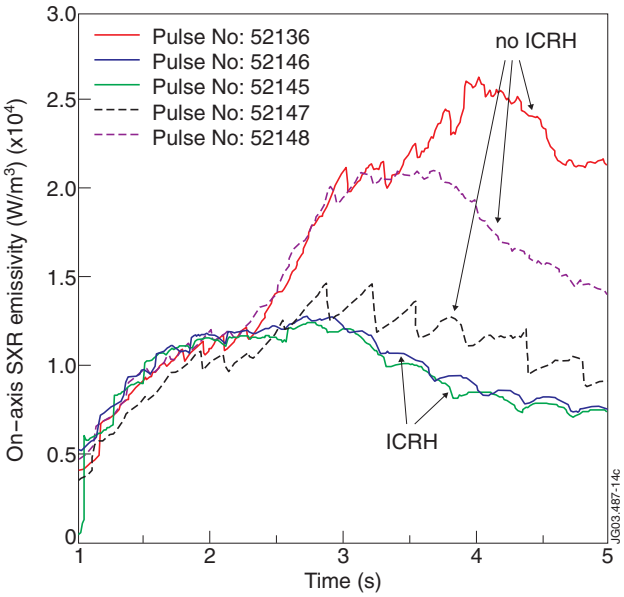

Figure 13: Comparison of the time evolution of the on-axis soft X-ray emissivity for 5 low triangularity discharges. The curves are numbered in order of increasing Ar injection rate (two numbers 3 indicate the same Ar influx).

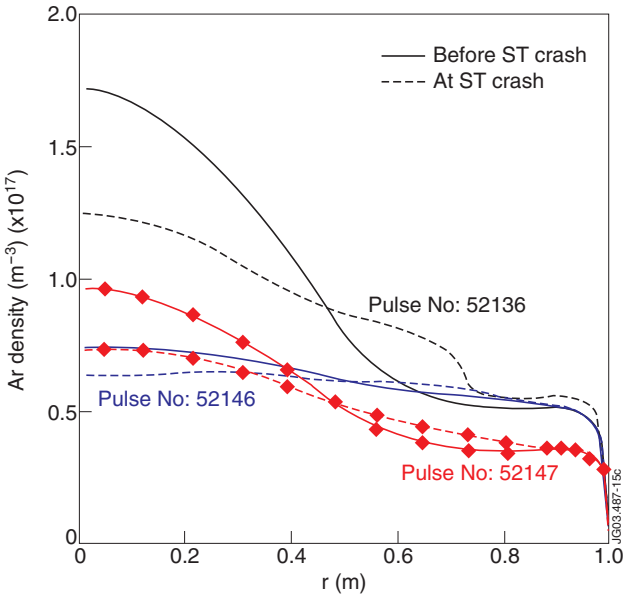

Figure 14: Effect of sawteeth during the after-puff phase in Pulse No's: 52146 (with ICRH), 52136 (without ICRH and 52147 (without ICRH and low Ar influx): calculated Ar density across a ST crash during the AP.

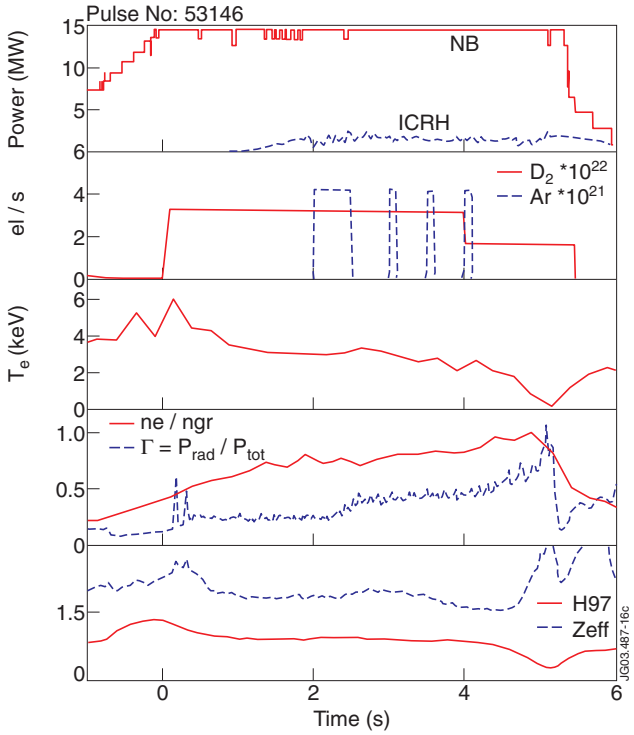

Figure 15: The same as fig.1 for the high triangularity Pulse No: 53146. From top to bottom: NB and RF Heating power, D_2 and Ar fluxes; on-axis electron temperature; radiation fraction (P_{rad}/P_{inp}) and Greenwald factor (n_e/n_{Gr}); effective charge and confinement factor f_{H97}. Times are referred to the start of Ar puff.

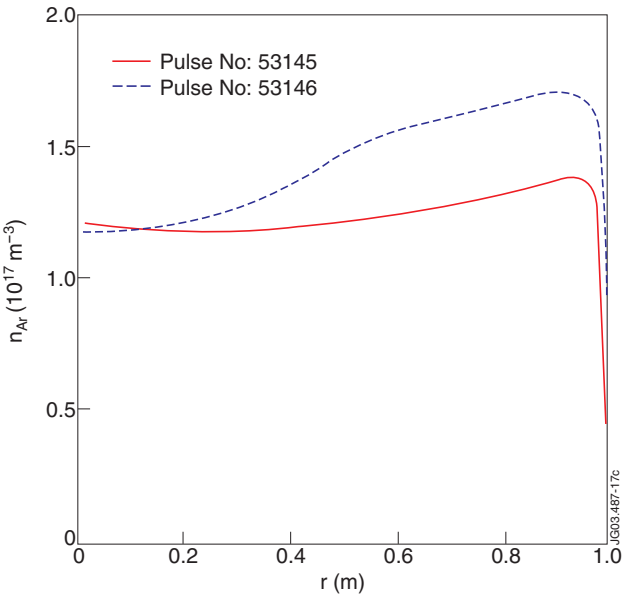

Figure 16: Ar density profiles for the high triangularity Pulse No's: 53146 (with ICRH) and 53145 (without ICRH). The Ar profiles are clearly flatter than in the low triangularity case (see Fig. 8).

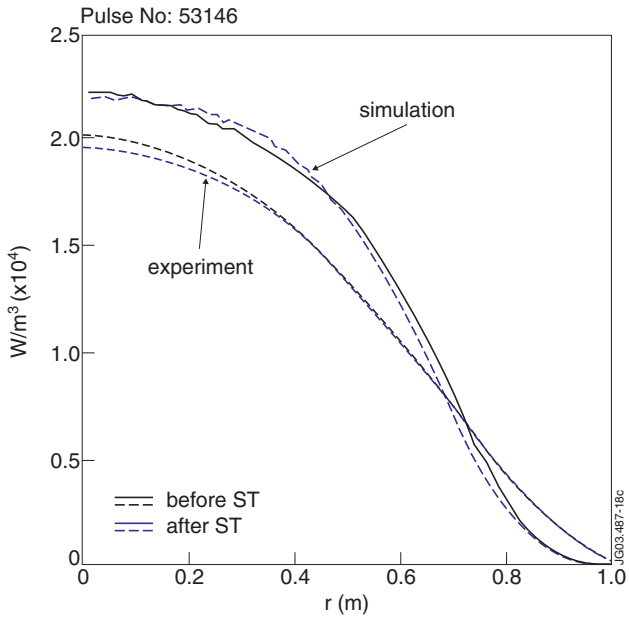

Figure 17: Effect of sawteeth in Pulse No: 53146: experimental and simulated soft X-ray emissivity profiles before and after a sawtooth.